TANGO1 assembles into rings around COPII coats at ER exit sites

Ishier Raote,[1,2] Maria Ortega Bellido,[1,2] Marinella Pirozzi,[3] Chong Zhang,[4] David Melville,[5] Seetharaman Parashuraman,[3] Timo Zimmermann,[1,2,6] and Vivek Malhotra[1,2,7]

[1]Centre for Genomic Regulation (CRG), The Barcelona Institute of Science and Technology, 08003 Barcelona, Spain
[2]Universitat Pompeu Fabra (UPF), 08002 Barcelona, Spain
[3]Institute of Protein Biochemistry, 80131 Naples, Italy
[4]SIMBIOsys Group, Department of Information and Communication Technologies, Universitat Pompeu Fabra (UPF), 08018 Barcelona, Spain
[5]Department of Molecular and Cellular Biology, Howard Hughes Medical Institute, University of California, Berkeley, Berkeley, CA 94720
[6]Advanced Light Microscopy Unit, Centre for Genomic Regulation (CRG), 08003 Barcelona, Spain
[7]Institució Catalana de Recerca i Estudis Avançats (ICREA), 08010 Barcelona, Spain

TANGO1 (transport and Golgi organization 1) interacts with CTAGE5 and COPII components Sec23/Sec24 and recruits ERGIC-53 (endoplasmic reticulum [ER]–Golgi intermediate compartment 53)–containing membranes to generate a mega-transport carrier for export of collagens and apolipoproteins from the ER. We now show that TANGO1, at the ER, assembles in a ring that encircles COPII components. The C-terminal, proline-rich domains of TANGO1 molecules in the ring are initially tilted onto COPII coats but appear to be pushed apart as the carrier grows. These findings lend support to our suggestion that growth of transport carriers for exporting bulky cargoes requires addition of membranes and not simply COPII-mediated accretion of a larger surface of ER. TANGO1 remains at the neck of the newly forming transport carrier, which grows in size by addition of ERGIC-53–containing membranes to generate a transport intermediate for the export of bulky collagens.

Introduction

Genetic and biochemical analyses of the process of formation of vesicular intermediaries at the ER and the Golgi complex have produced a detailed picture of molecular mechanisms involved in selective cargo export and retrieval at the ER (Bonifacino and Glick, 2004). However, an understanding of how these mechanisms are modulated to produce transport intermediates for sorting and export of bulky cargoes, such as collagen, remains elusive.

Identification of TANGO1 (transport and Golgi organization 1) as a functional and physical connection between cytoplasmic COPII coats and cargoes, such as collagens and apolipoproteins, in the lumen of the ER, permitted molecular analysis of the pathway by which cells export bulky secretory cargoes (Saito et al., 2009; Wilson et al., 2011; Malhotra and Erlmann, 2015; Santos et al., 2016). A cytoplasmic proline-rich domain (PRD) of TANGO1 has been shown to interact with ER exit site (ERES), COPII coat components, Sec23/Sec24 (Saito et al., 2009; Ma and Goldberg, 2016), whereas the interaction of TANGO1 with collagens requires an SH3-like domain of TANGO1 (Saito et al., 2009). Interestingly, the recent findings of Ishikawa et al. (2016) reveal that the SH3-like domain of TANGO1 binds the collagen-specific chaperone Hsp47. This

therefore helps explain the role of TANGO1 in the export of collagens in general from the ER. TANGO1 binds another ERES-resident protein, CTAGE5, which recruits Sec12, which in turn recruits more COPII coats (Saito et al., 2009, 2011, 2014). TANGO1 therefore has at least three major functions: it recruits and binds COPII coats; it recruits ER–Golgi intermediate compartment 53 (ERGIC-53)–containing membranes; and it binds Hsp47, which then collects procollagens.

It is not known how many fully folded and assembled triple helices of collagens can be exported in each transport carrier and whether such a carrier is engaged in the transport of only collagens or whether it also packages other small secretory cargoes. This is because carriers of collagens from the ER to the Golgi have not been characterized morphologically or biochemically.
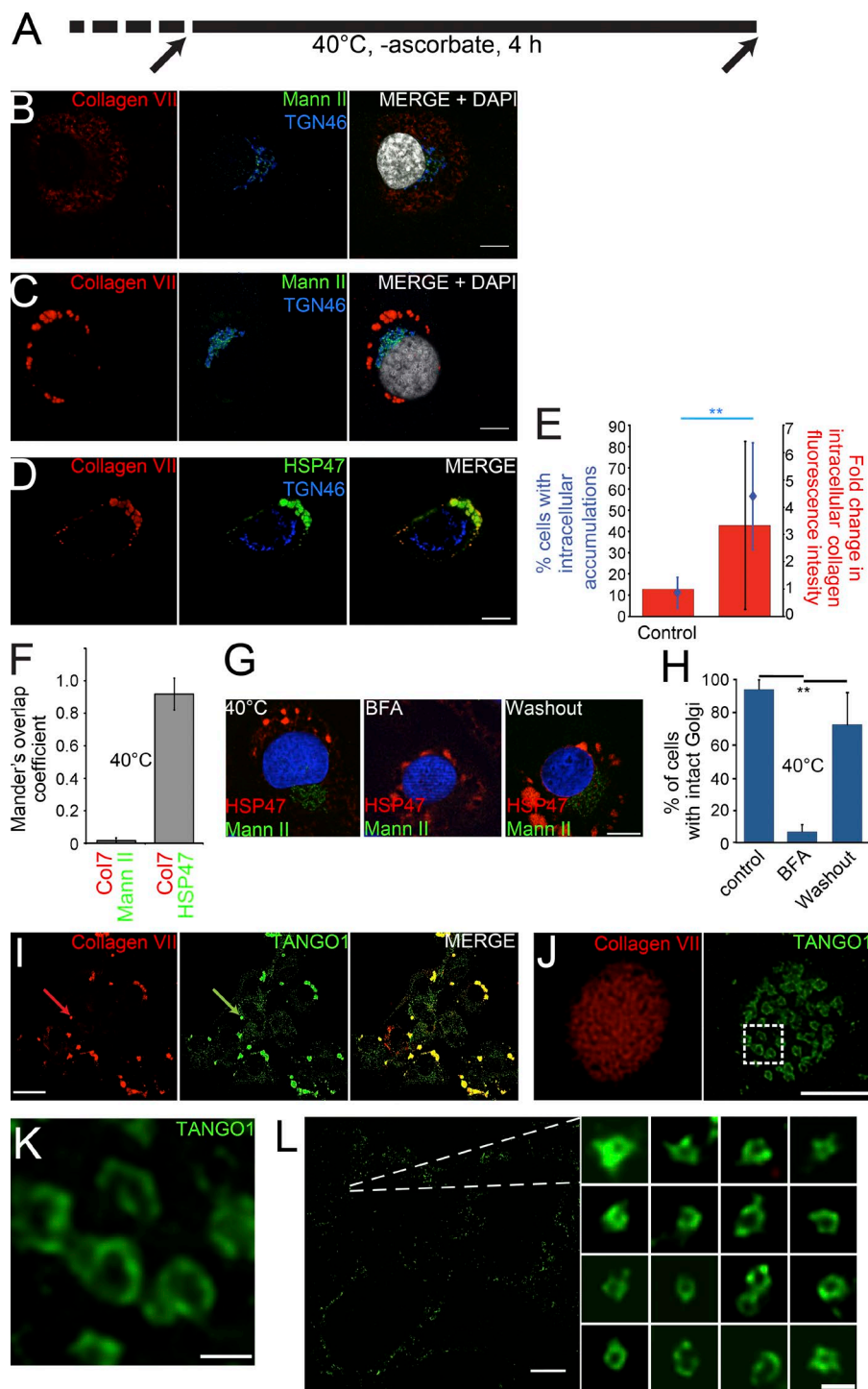
We have previously suggested that TANGO1 captures collagen in the lumen, which likely generates a collagen-enriched domain or a patch. ERGIC-53–containing membranes, recruited directly by TANGO1, fuse to this domain, providing membrane for the growth of a nascent bud and eventually a large carrier (Nogueira et al., 2014; Santos et al., 2015). But what is the functional organization of TANGO1

Check for updates

Figure 1. **TANGO1 assembles into a ring at patches of the ER enriched in collagen.** (A) Schematic of the protocol used to arrest collagen VII at the ER in RDEB/FB/C7 cells. Cells were grown at 37°C in complete medium, shifted to 40°C for 4 h in serum-free medium (Opti-MEM) lacking ascorbate, and then fixed and processed for immunofluorescence. (B) Cells at 37°C showed low levels of intracellular collagen VII (red). Mann II, mannosidase II. (C) When cells were shifted to 40°C in serum-free medium without ascorbate, collagen VII accumulated in intracellular patches (red). (D) Collagen VII intracellular patches colocalized with the ER-resident protein HSP47 (green). (E) This was accompanied by a threefold increase in fluorescence intensity of collagen VII staining (red bars). Accumulations of collagen VII were observed in nearly 60% of all cells in culture (blue diamonds). Values plotted are mean ± SD ($n = 5$). These accumulations were excluded from the Golgi complex, as marked by mannosidase II (C, green) or TGN46 (C and D, blue). (F) This was quantified using the Mander's overlap coefficients derived from images acquired of cells at 40°C, to look at the overlap between collagen VII (Col7) and either mannosidase II or HSP47 and plotted as mean ± SD. (G) Incubating cells at 40°C arrested collagen export. Cells were treated with BFA for 2 h and after that either fixed for imaging with anti–mannosidase II antibodies (BFA) or washed to remove BFA. After 2 h, these washed cells were fixed and visualized with anti–mannosidase II antibodies (washout). (H) The data were quantified ($n = 3$) and plotted here as mean ± SD. (I and J) Confocal image of a field of cells shows that these intracellular accumulations of collagen VII (I, red) recruit TANGO1 (I, green). A single accumulation (I, arrows) was imaged in STED mode (J, collagen VII in red and TANGO1 in green), and TANGO1 was resolved to clear rings (J, green). (K) Highlighted area of the super-resolution image of TANGO1 (boxed area in J) is magnified and shown. (L) CACO2 cells differentiated for 30 d were stained for TANGO1 and imaged in STED mode. Several distinct isolated spots of TANGO1 were resolved into rings and are shown magnified. Bars: (B–D and G) 10 µm; (I) 30 µm; (J) 3 µm; (K) 300 nm; (L) 5 µm; (L, insets) 200 nm. **, P ≤ 0.01, two-tailed Student's t test.

at this patch with respect to COPII coats and ERGIC membranes? Given the likely physical scales of these activities (probably no larger than 200 nm), conventional microscopy has proven inadequate to visualize their organization. However, recent advances in super-resolution microscopy now allow for a more comprehensive description of the organization of specific components at ERESs (Kurokawa et al., 2014; McCaughey et al., 2016) and how they might coordinate the export of collagen. Using stimulated emission depletion (STED) microscopy, we have addressed this key question and found to our surprise that TANGO1 is assembled in a ring that

surrounds COPII coats at the ER. The description and the significance of our findings follow.

Results and discussion

ER export of procollagen is inhibited at 40°C in medium lacking ascorbate

To characterize the functional organization of TANGO1 at an ERES, our first objective was to develop a cell system suitable to visualize this event, with high levels of TANGO1 and

collagen at the ER. To this end, we adapted a procedure previously used (Mironov et al., 2003) to inhibit procollagen export from the ER (depicted schematically in Fig. 1 A).

RDEB/FB/C7 cells (fibroblasts that stably express collagen VII), maintained at 37°C show low levels of intracellular collagen (Fig. 1 B, red), distributed throughout the ER, but after 4 h at 40°C in serum-free medium lacking ascorbate, collagen folding was inhibited and consequently arrested in the ER. This resulted in a threefold increase in levels of intracellular staining of collagen VII (quantified in Fig. 1 E) and in ∼60% of all cells (Fig. 1 E, blue diamonds) generated large accumulations of collagen VII (Fig. 1 C, red). Collagen VII accumulations (Fig. 1 C, red) are excluded from the Golgi complex (Fig. 1 C, green and blue, respectively). In these cells, procollagen VII accumulated in the ER, as can be seen by its colocalization (Fig. 1 D, red) with predominantly ER-localized collagen chaperone HSP47 (Fig. 1 D, green). Mander's overlap coefficients quantifying the overlap of collagen, HSP47, and mannosidase II are plotted in Fig. 1 F.

We confirmed that these conditions are not toxic to the cells used and that the ER remains fully functional in receiving from, and delivering membranes to, the Golgi apparatus. Evidence for this claim is based on the following data. We arrested collagen export from the ER by incubating cells at 40°C (Fig. 1 G). Cells were treated with brefeldin A (BFA) for 2 h to fuse Golgi membranes to the ER and, after that, either fixed for imaging with anti–mannosidase II antibodies (Fig. 1 G, BFA) or washed to remove BFA to regenerate Golgi apparatus (Fig. 1 G, washout). The data (quantified in Fig. 1 H) reveal that Golgi membranes fuse with the ER upon BFA treatment under conditions that block collagen export from the ER, and that the Golgi membranes exit the ER upon BFA removal, showing that the ER is functional with respect to receiving Golgi membranes and exporting membranes to produce a Golgi apparatus under conditions that block export of collagens.

These accumulations of collagen (Fig. 1 I, red) had two characteristic features that made them well suited for super-resolution microscopy. First, they were highly enriched in TANGO1 (Fig. 1 I, green), most of which would probably be bound to collagen, ensuring greater structural and functional homogeneity in complexes containing TANGO1. Second, they presented us with extensive planar surfaces ideal for microscopy, which facilitated an observation of TANGO1 with maximal lateral resolution and minimal axial contribution, as most TANGO1 would be perpendicular to the plane of the coverslip.

TANGO1 assembles into a ring

We visualized these accumulations with super-resolution STED microscopy using anti-TANGO1 and anti–collagen VII antibodies. Interestingly, we observed TANGO1 assembled in a ring-like configuration (Fig. 1, J and K, green) at accumulations of collagen. The collagen in these images, in many cases, also appeared in rings (Fig. 1 J). The significance of this organization of collagen with respect to TANGO1 is unclear. It is easy to envision that such a ringed structure would be missed around the edges of collagen patches, in sections of the ER that are not almost entirely flat, and at those exit sites where TANGO1 is not bound to its cargo.

Although these collagen-secreting fibroblasts are an excellent model system to study the organization of TANGO1, a potential concern was that this organization could be affected by collagen overexpression. To address this, we also visualized

TANGO1 in Caco-2 cells, the best available in vitro model of absorptive enterocytes. We have previously used this model system to show that secretion of another bulky cargo, chylomicrons, is also TANGO1 dependent (Santos et al., 2016). Caco-2 cells were differentiated for 30 d, and chylomicron secretion was induced as described previously (Santos et al., 2016). Cells were fixed with formaldehyde (4%) and immunostained with anti-TANGO1 antibody. Again, our observations revealed that TANGO1 was assembled into rings (Fig. 1 L, magnified insets). This suggests that the rings of TANGO are not an experimental artifact.

TANGO1 rings encircle budding COP II vesicles

We then visualized the organization of TANGO1 rings with respect to the localization of COPII coat components and ERGIC membranes at ERESts. In this experiment, we visualized collagen VII accumulations in RDEB/FB/C7 cells using an antibody against the outer-coat protein Sec31A (Fig. 2 A, red) along with TANGO1 (Fig. 2 A, green). Sec31A was found enclosed within rings of TANGO1 (Fig. 2 A, merge).

We have previously shown that TANGO1 directly recruits ERGIC membranes via a domain that we have named TEER (Santos et al., 2015). We therefore examined the localization of ERGIC membranes at the ring of TANGO1. RDEB/FB/C7 cells were stained with anti–ERGIC-53 (Fig. 2 B, red) and anti-TANGO1 (Fig. 2 B, green) antibodies, and we found that ERGIC-53 was organized differently than Sec31A, as it was excluded from within the circle formed by TANGO1. Gratifyingly, in accordance with our previously model of ERGIC-membrane recruitment, it was excluded from the center of the ring and restricted to the periphery or colocalized with TANGO1 in the ring-like conformation (Fig. 2 B, merge).

This result demonstrated that TANGO1 assembles into a ring at the base of a newly forming, Sec31-containing membrane domain. An attractive hypothesis is that the ring of TANGO1 serves as a "picket fence" to corral COPII coat components and act as a scaffold that recruits and stabilizes ERGIC membranes for use as building blocks for the production of a mega-carrier.

TANGO1 rings contract concomitantly with export of collagen from the ER

We next asked whether the rings of TANGO1 identify ERESts that are functional in the export of collagen. We hypothesized that because the rings are at the neck of a budding transport intermediate, the size of TANGO1 rings would shrink concomitantly with collagen export from the ER.

RDEB/FB/C7 cells that had been incubated at 40°C for 4 h were shifted to 32°C in the presence of 1 mM sodium ascorbate (schematically represented in Fig. 3 A) to promote the export of folded and assembled collagens from the ER (Mironov et al., 2003). To verify that collagen VII was exported from the ER under these conditions, cells were fixed after 30 min and visualized by confocal microscopy using antibodies against collagen VII (Fig. 3 B, red), along with ER marker calreticulin (green) and the Golgi complex resident protein TGN46 (blue). At this time point, a pool of collagen VII was seen that no longer colocalized with calreticulin but rather converged on TGN46 (Fig. 3 B, blue arrow). We predicted that there would be TANGO1-dependent collagen carriers in various stages of biogenesis, which would result in a shift of the distribution of size of TANGO1 rings toward smaller rings.
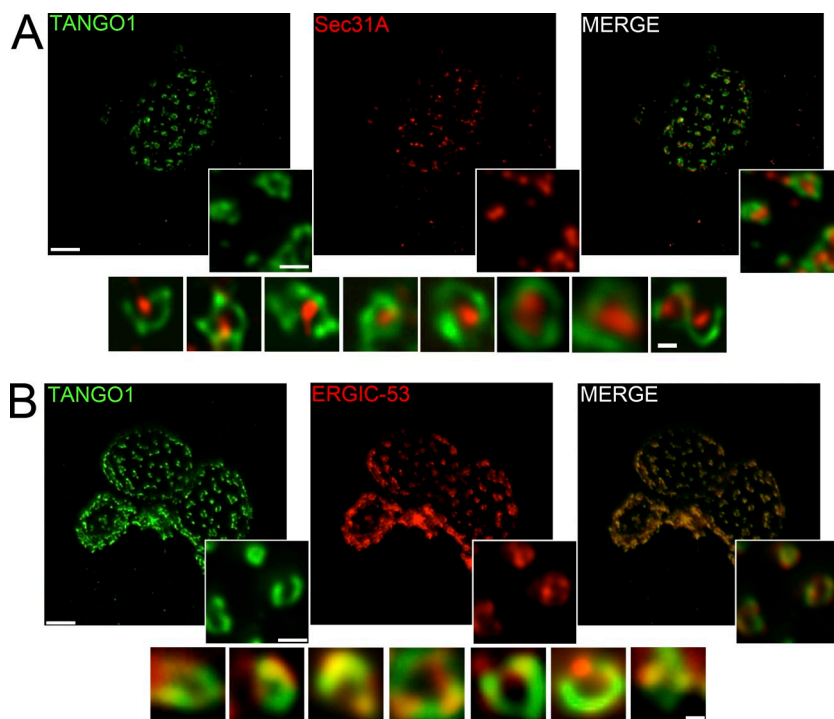
Figure 2. **TANGO1 rings encircle vesicles budding from the ER.** (A) RDEB/FB/C7 cells incubated at 40°C and stained with anti-TANGO1 (green) and anti-Sec31A antibodies (red), showing Sec31A encircled by TANGO1 rings (merge). (B) Cells were stained with anti-TANGO1 (green) and anti–ERGIC-53 (red) antibodies. ERGIC membranes were excluded from the center of the ring (merge), instead appearing at the periphery, alongside TANGO1. (A and B) Insets are magnifications of a part of the same image. Bars: (A and B) 1 µm; (insets) 200 nm; (panel of insets) 100 nm.

Super-resolution images of rings of TANGO1 were obtained from these cells incubated for 4 h at 40°C (Fig. 3 C, t0') or after shifting cells to 32°C for 30 min (Fig. 3 C, t30'). We measured the mean diameters of TANGO1 rings at 40°C and 32°C in ascorbate-treated cells. From these images, we extracted parameters that we used to describe the size and shape of rings of TANGO1, as described in Materials and methods. In brief, diameters were extracted in two ways: either after fitting observed structures to an ellipse and determining major and minor axes or by measuring the length and breadth of a bounding rectangle (Feret's major/minor axes, respectively) around TANGO1 structures. It is clear that TANGO1 was found in rings under both of these experimental conditions. Interestingly, however, concomitant with collagen export from the ER, there was a detectable reduction in the mean size of TANGO1 rings, as shown in Fig. 3 D (*, P < 0.06; ***, P < 0.006). This change in the diameter of TANGO1 rings was not accompanied by a change in shape, as depicted in the measured aspect ratio of the diameters on the axes of the fitted ellipse (Fig. 3 E; ns, not significant). The measured effect was perforce minimal as we were close to the limit of resolution of these structures. Although the significance of this change in ring diameter is not obvious, we speculate that it could represent a step in the constriction of the neck in events leading to the separation of a collagen-filled bulky transport carrier from the ER. The sizes as determined by each of these parameters are detailed in tabular form (Fig. 3 F).

These data provided evidence that TANGO1 rings marked functional budding collagen carriers. Our elementary analysis of TANGO1 rings provided an immediate important insight into the packaging of collagens: a fully assembled, rigid, triple-helical collagen trimer is far larger than the ring and therefore must be exported from the ER into a carrier end-on, in an orientation perpendicular to the ER membrane. Additionally, because TANGO1 is a constraint at the base of the vesicle, it is ideally localized to recruit membrane constriction and scission machinery and delimit its area of activity. It would therefore be interesting to see what roles TANGO1 plays in the process of membrane fission.

The C-terminal PRD of TANGO1 overlies the COPII coats encased by a TANGO1 ring

We have shown before by yeast two-hybrid that the PRD of TANGO1 interacts with Sec23/Sec24 of COPII coats (Saito et al., 2009). There is now biochemical and structural evidence for the interaction between the PRD of TANGO1 with COPII component Sec23 (Ma and Goldberg, 2016). What then is the organization of the PRD of TANGO1 with respect to the ring of TANGO1?

We hypothesized that, using antibodies that target distinct spatially separated sites on TANGO1, we might be able to visually distinguish the organization of cytoplasmic and lumenal portions of TANGO1 with respect to each other. To this end, we generated a TANGO1 construct with an HA-epitope placed at the C terminus of the PRD (T1-HA). A schematic representation of the construct and the two sites recognized by antibodies is depicted in Fig. 4 A.

We then tested the localization of this TANGO1 construct in HeLa cells. We had previously generated a cell line (denoted 2H5) derived from HeLa cells from which TANGO1 was deleted using the CRISPR/Cas9 system (Santos et al., 2015). 2H5 cells were cotransfected with full-length wild-type T1-HA and collagen VII. 2H5-T1-HA cells were stained with anti-TANGO1 antibody and visualized by STED microscopy. The results revealed that TANGO1 is recruited to accumulations of collagen VII, and as seen in RDEB/FB/C7 cells, the arrangement of TANGO1 is in rings (Fig. 4 B, green) that encircle Sec31 (Fig. 4 B, green, merge).

Cells expressing these constructs were immunostained using anti–HA-epitope antibody and anti-TANGO1 antibody. The lumenal epitope appears ring-like, but interestingly, the C terminus (PRD) was seen in two distinct configurations. In one conformation, it was visualized like Sec31: in a
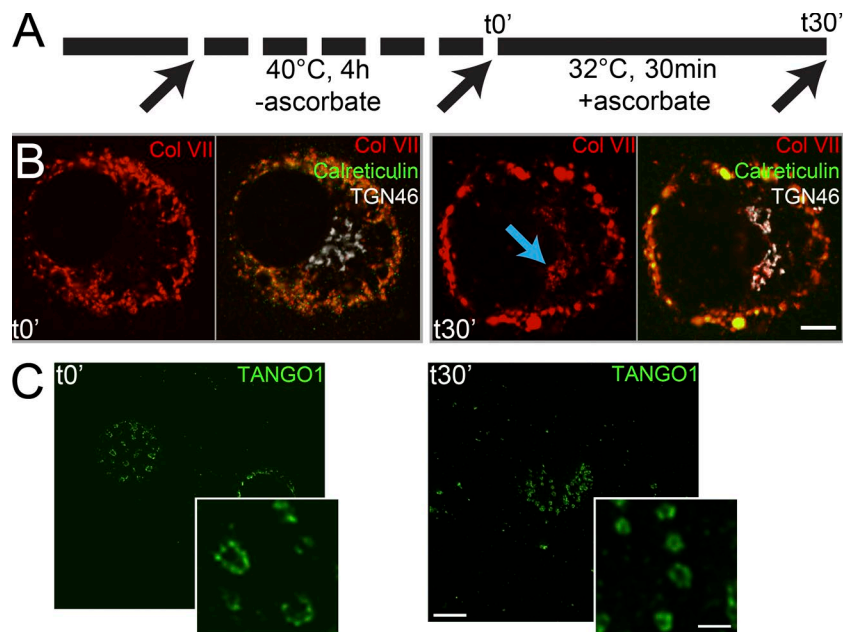
Figure 3. **TANGO1 rings shrink concomitantly with collagen export from the ER.** (A) Schematic of the protocol followed in promoting collagen export from the ER. (B) Confocal images showing collagen VII (Col VII) trapped in the ER (t0' red); when cells were shifted to 32°C with added ascorbate for 30 min, (t30'), there was a pool of collagen VII (red) around the Golgi complex (t30' blue arrow), which no longer colocalized with the ER marker calreticulin (t30' merge). (C) STED imaging shows that TANGO1 assembled into rings at both time points (t0' and t30'). Insets are magnifications of a part of the same image. (D) Quantification of size, shown as scatter plot and box plot of measured morphological descriptors: major and minor axes, diameter of fitted ellipse, and maximum and minimum of Feret's diameter. (E) Quantification of shape, shown as scatter plot and box plot of measured aspect ratio between major and minor axes and diameter of the fitted ellipse. The number of rings analyzed for the two independent experiments are indicated (146 and 145, respectively). Mean and SD values of measurements plotted in D and E and tabulated in F. *, P < 0.06; ***, P < 0.006; ns, not significant. Bars: (B) 10 µm; (C) 2 µm; (C, insets) 400 nm.

F
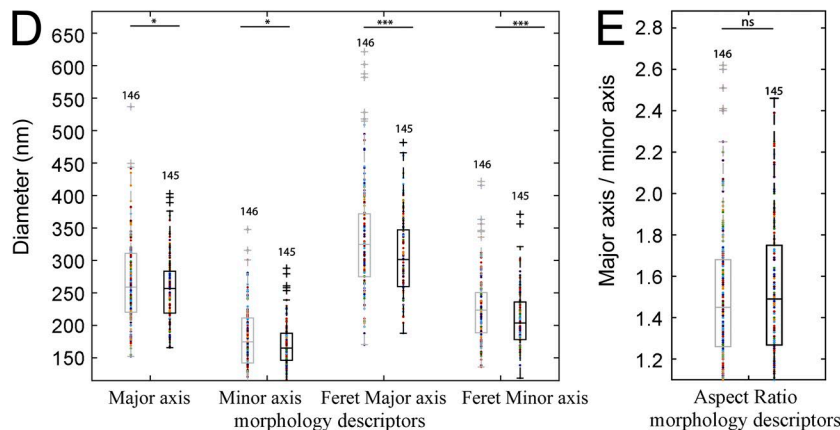
		Major axis	Minor axis	Feret Major axis	Feret Minor axis
t0'	Mean	268	181.1	331.9	225.4
	SD	68.9	44.6	86.9	53.2
t30'	Mean	254.9	170.3	305.7	209.9
	SD	49.4	34.4	63.2	41.7

punctum, completely encircled by the ring of TANGO1. Alternatively, in some cases, the C terminus of TANGO1 also formed a ring (Fig. 4, C and higher magnification in D, red) that neatly overlaid the ring described by the lumenal antibody (Fig. 4, C and higher magnification in D, green, merge). This strongly suggested that there were two distinct conformations adopted by the PRD in conjunction with the organization of COPII coats that could represent different stages during the biogenesis of a carrier at the ER. We hypothesized that the conformation with the C termini of TANGO1 in a punctum represented an early stage of the biogenesis of the carrier, as the carrier was still small enough for TANGO1 to overlay the COPII coats. As this budding vesicle grew, the TANGO1 molecules assembled in the ring were pushed upright and apart, such that the C termini were now localized to the periphery of the ring demarcated by the lumenal TANGO1 antibody, surrounding this larger nascent vesicle. Importantly, using STED microscopy, we have distinguished

between two molecular conformations of a single complex during the process of vesicle biogenesis.

Based on this new data, we present a working hypothesis of the spatiotemporal sequence of TANGO1's function in the export of collagens (as shown in Fig. 5). It is known that TANGO1 binds cTAGE5 on the cytoplasmic side. cTAGE5 does not have the lumenal cargo–interacting domain but does contain a PRD that, like TANGO1, binds Sec23 of Sec23/Sec24 inner-coat complex. For the sake of simplicity, however, we show only TANGO1 with respect to COPII coats in the events leading to the formation of collagen-containing carriers.

Steady state. TANGO1 binds Sec23/Sec24 via interaction of the PRD and Sec23 in Sec23/Sec24 complex. This binding is likely weak, which allows Sec13/Sec31 to come on and off Sec23/Sec24. Binding of TANGO1 to collagen in the lumen shifts the equilibrium by increasing binding of TANGO1 PRDs to Sec23. We expect that under steady-state conditions, there are two different complexes of Sec23/Sec24, one bound to
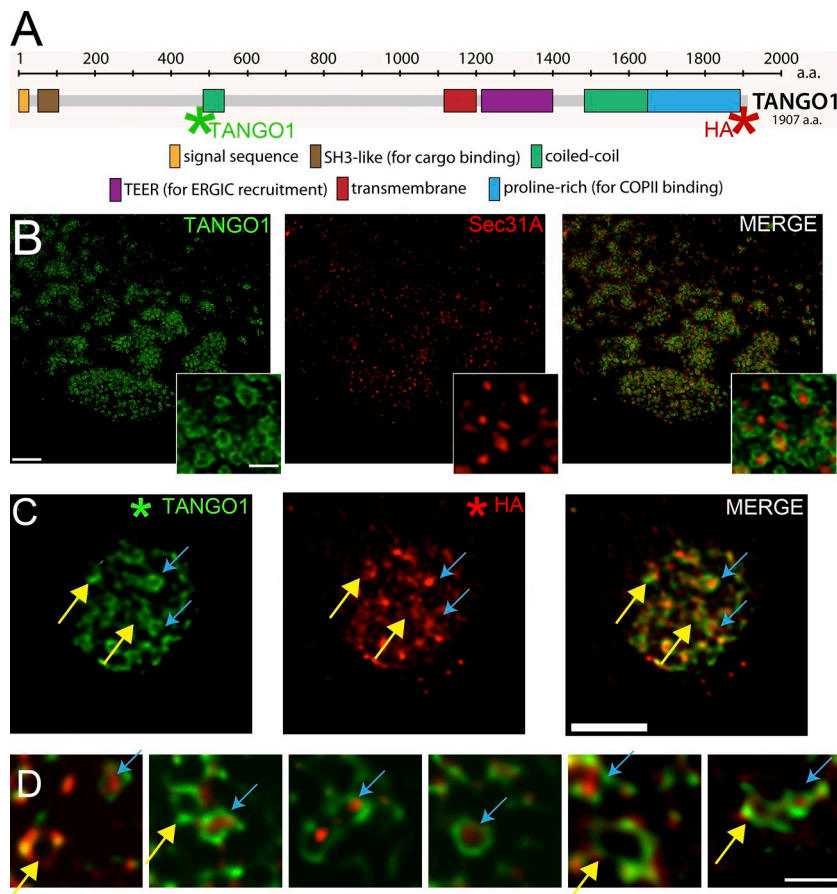
Figure 4. **TANGO1 rings can be visualized in two distinct conformations.** (A) Schematic showing the domain architecture of the TANGO1-HA construct used, indicating specifically the sites that are targeted by the two antibodies used (green asterisk, anti-TANGO1; red asterisk, anti-HA). (B) TANGO1-HA was expressed in HeLa cells lacking endogenous TANGO1; the exogenously expressed TANGO1-HA formed rings (green). Sec31A was encircled within the ring formed by TANGO1 (red, merge). Insets are magnifications of a part of the same image. (C and D) When cells were stained with anti-TANGO1 (green) and anti-HA epitope antibodies (red), either the HA was in the middle of the ring formed by anti-TANGO1 (C, blue arrows in red and merge) or at the perimeter of the ring (D, blue arrows in red and merge). Bars: (A) 2 µm; (B and C) 1 µm; (B and C, insets) 400 nm.

PRD of TANGO1 and another bound to Sec13/Sec31. However, even with super-resolution microscopic procedures used here, we cannot resolve these two complexes within the ring of TANGO1. This explains our data that PRD appears within the TANGO1 ring (when bound to Sec23) and in the ring surrounding the coats (unbound to Sec23). This explains the two distinct organizations of the PRD of TANGO1 with respect to Sec31 (Fig. 5).

Stage I–II. Binding to collagen in the lumen increases the avidity of TANGO1 to Sec23. ERGIC-53–containing membranes recruited by TEER domain of TANGO1 fuse within the TANGO1 ring, and this extra membrane is rapidly consumed into the growing carrier. During this process, TANGO1 can only extend a maximum of 30–50 nm (estimated from the presence of two coiled domains in the cytoplasmic domain of each)
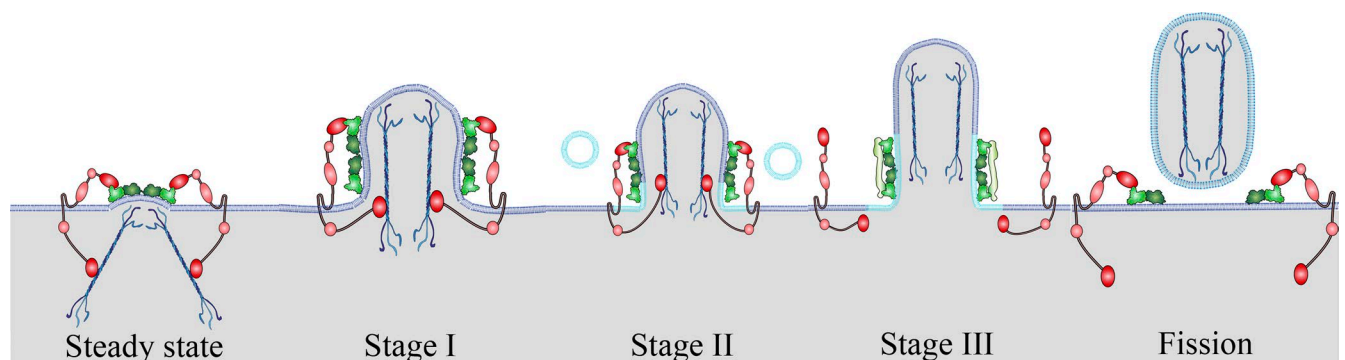
Figure 5. **TANGO1 organization in the export of collagen from the ER.** Under steady state, Sec23/Sec24 exists in two complexes: bound to PRD of TANGO1 (not depicted in the diagram is cTAGE5 that is bound to TANGO1, contains PRD, but lacks the lumenal cargo–binding domain) or to Sec13/Sec31. For the sake of simplicity, only Sec23/Sec24 is shown here. TANGO1 interacts with collagen via Hsp47 bound to the lumenal SH3-like domain. The PRD is oriented inward, overlaying the inner COPII coat proteins and also in the ring of TANGO1. Stages I and II represent the initial growth by pushing of collagen against the lumenal face of the ER (II) and fusion of ERGIC-53–containing membranes. We expect that parts of this tubule-like structure are coated with both Sec23/Sec24 and Sec13/Sec31. However, TANGO1 remains bound to Sec23 in the Sec23/Sec24 complex and fixed at the neck of the growing tubule. Stage III corresponds to the growth of tubule that is large enough to accommodate collagens. Once this has been achieved, the separation of SH3-like domain from Hsp47 collagens in the lumen triggers the release of PRD from Sec23. This then follows the recruitment of Sec13/Sec31 to Sec23/Sec24 at the neck of the collagen-filled tubule. Sec31-mediated activation of Sar1-GTP hydrolysis by Sec23 then leads to membrane fission to separate a collagen-filled container from the ER (separation stage).

perpendicular to the plane of the ER. TANGO1 bound to Sec23/Sec24 therefore remains at the neck of the growing tubule. The growing tip of this tubule, we expect, might in fact be coated by both Sec23/Sec24 and Sec13/Sec31, the latter being carried over into the growing tubules from the distribution of the two complexes Sec23/Sec24 (described in Steady state).

Stage III–IV. This growth of the carrier continues until collagen trimers are completely encased in a tubule commensurate with the length of a fully assembled collagen trimer, which in the case of collagen VII might reach greater than 450 nm. Dissociation of collagen, Hsp47, and TANGO1 releases TANGO1 from Sec23/Sec24, followed by recruitment of Sec13/Sec31 to the neck of the carrier (Fig. 5).

Separation by membrane fission. The binding of Sec13/Sec31 to Sec23/Sec24 initiates Sar1-GTP hydrolysis and membrane fission, leading to separation of a collagen-filled tubule from the ER (Fig. 5).

Thus, TANGO1 appears to function as a modular protein, with at least three distinct portions performing independent functions in each stage of the overall process of vesicle biogenesis and cargo export from the ER. One, it binds Hsp47, which in turn binds collagens in the lumen of the ER. Two, the cytoplasmic portion of TANGO1 corrals coat components and modulates the interactions between the inner- and outer-coat proteins to control Sec31-mediated activation of Sec23-catalyzed Sar1-GTP hydrolysis, thereby controlling the timing of membrane fission. Three, by tethering the ERES to the ERGIC, TANGO1 provides a rapid means to grow a transport carrier commensurate with cargo size and improve the efficiency of cargo transfer from the ER to the next destination along the secretory pathway.

It is not unreasonable to suggest that this modular form and function of TANGO1 serves to link the folding propensity of cargoes and their size to their export by controlling growth of the respective carriers. Cargoes such as collagens, chylomicrons, and other proteins that require extensive assistance in folding and assembly are selected by TANGO1 in the lumen and connected to the cytoplasmic machinery to ensure generation of carriers that fit the cargo. The lumenal unstructured portion of TANGO1 likely plays a crucial role as a scaffold in the overall assembly of folded complex cargoes. Recruitment of ERGIC membranes by TANGO1 is a vast source of membranes (building blocks) for rapid growth of the carrier. In simple terms, TANGO1 is part of the quality control mechanism that links folding and assembly of complex molecules to their export by carriers of the right size. That these functions may be at least partly independent is indicated by the observation that TANGO1-short (an isoform of TANGO1 lacking lumenal domains) can partially compensate for a loss of full-length TANGO1 (Maeda et al., 2016). In this instance, we suggest that overexpressed TANGO1-short interacts with Sec23 and also recruits ERGIC-53 membranes, thus facilitating the growth of the carrier and sustaining cargo export, albeit inefficiently. It is important to note that TANGO1 in flies also assembles into rings (see Liu et al., 2017, companion paper in this issue). However, unlike mammals, which express TANGO1, cTAGE5, TANGO1-short, and TALI, flies express only TANGO1. It is therefore likely that loss of TANGO1, by affecting recruitment of ERGIC-53–containing membranes, would reduce the size and/or number of vesicles generated at the ERES. Because collagens are the most abundant secretory cargoes, affecting this major export pathway will consequently have an effect on the export of other, smaller, secretory cargoes. This is certainly likely to be the case for many exogenously expressed, nonnatural secretory proteins, such as signal sequence (ss)–luciferase, ss-GFP, and ss-HRP. In mammals, this might also be the case, but the presence of TANGO1 and TANGO-like proteins and isoforms strongly suggests that their involvement in the export of other secretory cargoes is secondary to their main role in the export of bulky and difficult-to-fold/assemble cargoes such as collagens and apolipoprotein B–containing lipoproteins.

Materials and methods

Cell culture
RDEB/FB/C7 and HeLa cells were grown at 37°C with 5% CO_2 in complete DMEM with 10% FBS unless otherwise stated. Plasmids were transfected in HeLa cells with TransIT-HeLaMONSTER (Mirus Bio LLC) or Lipofectamine 3000 Transfection Reagent (Thermo Fisher Scientific) according to the manufacturer's protocols. Caco-2 cells were grown as described previously (Santos et al., 2016). In brief, Caco-2 cells were grown in complete DMEM with 20% FBS for 30 d to differentiate, with changes to fresh medium every 2 d. To induce chylomicron/very-low-density lipoprotein (VLDL) secretion, FCS-free medium with oleic acid (1.5 mM; Sigma-Aldrich) solubilized in fatty acid–free BSA (Sigma-Aldrich) was added to the cells for 5 h.

Antibodies
The following antibodies were used in immunocytochemistry: collagen VII (rabbit anti–human [Abcam]; mouse anti–human [Sigma-Aldrich]), ERGIC-53 (mouse anti–human; Santa Cruz Biotechnology, Inc., and Enzo Life Sciences), Sec31A (mouse anti–human; BD), TANGO1 (rabbit anti–human; Sigma-Aldrich), HSP47 and calreticulin (goat anti–human; Enzo Life Sciences), HA (mouse; BioLegend), SAR1 (mouse anti–human; Abcam), TGN46 (Bio-Rad Laboratories), and mannosidase II (rabbit anti–human; Bio-Rad Laboratories and Merck). Mounting media used in confocal and STED microscopy were either Vectashield (Vector Laboratories) or ProLong (Thermo Fisher Scientific).

Immunofluorescence microscopy
Cells grown on coverslips were fixed with cold methanol for 8 min at −20°C or 4% formaldehyde (Ted Pella, Inc.) for 15 min at room temperature. Cells fixed with formaldehyde were permeabilized with 0.1% Triton in PBS and then incubated with blocking reagent (Roche) for 30 min at room temperature. Primary antibodies were diluted in blocking reagent and incubated overnight at 4°C or at 37°C for 1 h. Secondary antibodies conjugated with Alexa Fluor 594, 488, or 647 were diluted in blocking reagent and incubated for 1 h at room temperature.

Confocal images were taken with a TCS SP5 (63×, 1.4–0.6 NA, oil, HCX PL APO), TCS SP8 (63×, 1.4 NA, oil, HC PL APO CS2), or TCS SPE (63×, 1.3 NA, oil, ACS APO; all from Leica Microsystems) using Leica acquisition software. Lasers and spectral detection bands were chosen for the optimal imaging of Alexa Fluor 488, 594, and 647 signals. Two-channel colocalization analysis was performed using ImageJ (National Institutes of Health), and the Mander's correlation coefficient was calculated using the plugin JaCop (Bolte and Cordelières, 2006).

STED microscopy
Confocal and STED images were taken on a TCS SP8 STED 3× microscope (Leica Microsystems) on a DMI8 stand using a 100× 1.4-NA oil HCS2 PL APO objective and a pulsed supercontinuum light source (white light laser). Images were acquired at a pixel size of 19.79 nm

for super-resolution imaging. The STED settings were chosen to maximally improve lateral resolution (0% 3D STED). Images of Alexa Fluor 594 were taken with 580-nm excitation and emission detection between 590 and 640 nm. For STED imaging, a picosecond pulsed depletion laser at 775 nm was added with a 0-ps pulse delay at 80% intensity. Confocal images were taken with 1× line integration and 3× frame means; STED images were taken with 8× line integration and 3× frame means. Images of Atto647N or Abberior 635 were taken with 655-nm excitation and emission detection between 660 and 748 nm. For STED imaging, a pulsed depletion laser at 775 nm was added with 0-ps pulse delay at 30% intensity. Confocal images were taken with 1× line integration and 3× frame means; STED images were taken with 8–14× line integration and 2–3× frame means. The channels of 3D stacks were taken sequentially in a frame-by-frame acquisition mode.

The accurate determination of STED image resolution in the samples is generally difficult, as it depends on the power of the depletion beam and the quality of the alignment of the depletion doughnut, which may be negatively affected by properties of the sample (refractive index of the mounting medium, coverslip properties, distance of imaged area from the coverslip, etc.) as well as the intrinsic fluorophore properties in the sample environment. Care was taken to optimize all these aspects, but in the absence of a small structure of known size in the sample, the resolution can best be defined by determining the smallest detectable structures in the image datasets. These were identified by appearing in several z-slices of the dataset (to avoid measuring random fluctuations) and were found to be ∼60 nm for the Atto647N/Abberior 635 channel and 50 nm for the Alexa Fluor 594 channel. These are expected values for STED imaging with the powers and detection settings used and are small enough to resolve and measure the described TANGO structures. The slightly better resolution of the Alexa Fluor 594 channel is the result of a higher amount of depletion used for this channel, as both channels were set up to minimize bleaching to allow repeated imaging for the acquisition of z-stacks.

Because of the small size of the described structures, no attempt has currently been made to resolve ring structures in the axial direction by 3D STED, and only structures suitably oriented in the image plane were analyzed. This allows us to fully use the improved lateral resolution in the x/y STED regimen but does not improve axial resolution beyond what is possible by optical diffraction. Improving axial resolution by applying STED in z would degrade lateral resolution while still not reaching sufficient resolution for axially oriented structures, especially as full depletion powers would fully bleach the sample during the acquisition of the required z-information (which would need to be taken with step sizes <<100 nm). As sample illumination is inevitably axial, xz-scanning would not help the issue.

For the acquisition and analysis of laterally oriented structures, z-stacks were taken at 100-nm steps to obtain sufficient z-sampling for subsequent deconvolution. The settings for the deconvolution were chosen to improve structure contrast and reduce image noise while not changing the size of the smallest detected structures (50–60 nm).

Morphology quantification of TANGO1 rings

Multichannel 3D stacks were acquired with a z-step size of 100 nm and subsequently deconvolved using Huygens deconvolution software (Scientific Volume Imaging) for STED modes using shift correction to account for drift during stack acquisition. Maximum-intensity projections were then generated from a subset of the deconvolved stack slices where the rings were present. The rings were segmented via a semiautomatic procedure of thresholding and post-processing of non-ring–like objects. The size and shape of each segmented ring were quantified with ImageJ. Specifically, we measured the diameters of the ring in terms of major and minor axes of its fitted ellipse and the maximum and minimum

Feret's diameter. Statistical testing was performed using Student's t test (continuous data, two groups). One asterisk indicates Student's t test value $P < 0.06$; three asterisks $P < 0.006$; ns indicates not significant.

Author contributions: I. Raote: conceptualization, formal analysis, investigation, validation, methodology, project administration, visualization, and writing (draft preparation, review, and editing). M. Ortega Bellido: investigation, validation, resources, and project administration. M. Pirozzi: investigation and formal analysis. C. Zhang: formal analysis and resources. D. Melville: visualization. S. Parashuraman: resources and formal analysis. T. Zimmermann: formal analysis and resources, software. V. Malhotra: conceptualization, funding acquisition, project administration, supervision, and writing (draft preparation, review, and editing).

References

Bolte, S., and F.P. Cordelières. 2006. A guided tour into subcellular colocalization analysis in light microscopy. *J. Microsc.* 224:213–232. http://dx.doi.org/10.1111/j.1365-2818.2006.01706.x

Bonifacino, J.S., and B.S. Glick. 2004. The mechanisms of vesicle budding and fusion. *Cell.* 116:153–166. http://dx.doi.org/10.1016/S0092-8674(03)01079-1

Ishikawa, Y., S. Ito, K. Nagata, L.Y. Sakai, and H.P. Bächinger. 2016. Intracellular mechanisms of molecular recognition and sorting for transport of large extracellular matrix molecules. *Proc. Natl. Acad. Sci. USA.* 113:E6036–E6044. http://dx.doi.org/10.1073/pnas.1609571113

Kurokawa, K., M. Okamoto, and A. Nakano. 2014. Contact of cis-Golgi with ER exit sites executes cargo capture and delivery from the ER. *Nat. Commun.* 5:3653. http://dx.doi.org/10.1038/ncomms4653

Liu, M., Z. Feng, H. Ke, Y. Liu, T. Sun, J. Dai, W. Cui, and J.C. Pastor-Pareja. 2017. Tango1 spatially organizes ER exit sites to control ER export. *J. Cell Biol.* 216. http://dx.doi.org/10.1083/jcb.201611088

Ma, W., and J. Goldberg. 2016. TANGO1/cTAGE5 receptor as a polyvalent template for assembly of large COPII coats. *Proc. Natl. Acad. Sci. USA.* 113:10061–10066. http://dx.doi.org/10.1073/pnas.1605916113

Maeda, M., K. Saito, and T. Katada. 2016. Distinct isoform-specific complexes of TANGO1 cooperatively facilitate collagen secretion from the endoplasmic reticulum. *Mol. Biol. Cell.* 27:2688–2696. http://dx.doi.org/10.1091/mbc.E16-03-0196

Malhotra, V., and P. Erlmann. 2015. The pathway of collagen secretion. *Annu. Rev. Cell Dev. Biol.* 31:109–124. http://dx.doi.org/10.1146/annurev-cellbio-100913-013002

McCaughey, J., V.J. Miller, N.L. Stevenson, A.K. Brown, A. Budnik, K.J. Heesom, D. Alibhai, D.J. Stephens 2016. TFG promotes organization of transitional ER and efficient collagen secretion. *Cell Reports.* 15:1648–1659. http://dx.doi.org/10.1016/j.celrep.2016.04.062

Mironov, A.A., A.A. Mironov Jr., G.V. Beznoussenko, A. Trucco, P. Lupetti, J.D. Smith, W.J.C. Geerts, A.J. Koster, K.N.J. Burger, M.E. Martone, et al. 2003. ER-to-Golgi carriers arise through direct en bloc protrusion and multistage maturation of specialized ER exit domains. *Dev. Cell.* 5:583–594. http://dx.doi.org/10.1016/S1534-5807(03)00294-6

Nogueira, C., P. Erlmann, J. Villeneuve, A.J. Santos, E. Martínez-Alonso, J.A. Martínez-Menárguez, and V. Malhotra. 2014. SLY1 and Syntaxin 18 specify a distinct pathway for procollagen VII export from the endoplasmic reticulum. *eLife.* 3:e02784. http://dx.doi.org/10.7554/eLife.02784

Saito, K., M. Chen, F. Bard, S. Chen, H. Zhou, D. Woodley, R. Polischuk, R. Schekman, and V. Malhotra. 2009. TANGO1 facilitates cargo loading at endoplasmic reticulum exit sites. *Cell.* 136:891–902. http://dx.doi.org/10.1016/j.cell.2008.12.025

Saito, K., K. Yamashiro, Y. Ichikawa, P. Erlmann, K. Kontani, V. Malhotra, and T. Katada. 2011. cTAGE5 mediates collagen secretion through interaction with TANGO1 at endoplasmic reticulum exit sites. *Mol. Biol. Cell.* 22:2301–2308. http://dx.doi.org/10.1091/mbc.E11-02-0143

Saito, K., K. Yamashiro, N. Shimazu, T. Tanabe, K. Kontani, and T. Katada. 2014. Concentration of Sec12 at ER exit sites via interaction with cTAGE5 is required for collagen export. *J. Cell Biol.* 206:751–762. http://dx.doi.org/10.1083/jcb.201312062

Santos, A.J.M., I. Raote, M. Scarpa, N. Brouwers, and V. Malhotra. 2015. TANGO1 recruits ERGIC membranes to the endoplasmic reticulum for procollagen export. *eLife.* 4:4. http://dx.doi.org/10.7554/eLife.10982

Santos, A.J.M., C. Nogueira, M. Ortega-Bellido, and V. Malhotra. 2016. TANGO1 and Mia2/cTAGE5 (TALI) cooperate to export bulky pre-chylomicrons/VLDLs from the endoplasmic reticulum. *J. Cell Biol.* 213:343–354. http://dx.doi.org/10.1083/jcb.201603072

Wilson, D.G., K. Phamluong, L. Li, M. Sun, T.C. Cao, P.S. Liu, Z. Modrusan, W.N. Sandoval, L. Rangell, R.A. Carano, et al. 2011. Global defects in collagen secretion in a Mia3/TANGO1 knockout mouse. *J. Cell Biol.* 193:935–951. http://dx.doi.org/10.1083/jcb.201007162